Synergistic Effects of the Membrane Actions of Cecropin-Melittin Antimicrobial Hybrid Peptide BP100

Rafael Ferre,[†] Manuel N. Melo,[‡] Ana D. Correia,[‡] Lidia Feliu,[†] Eduard Bardají,[†] Marta Planas,[†] and Miguel Castanho[‡*]

[†]Laboratori d'Innovació en Processos i Productes de Síntesi Orgànica, Departament de Química, Universitat de Girona, Girona, Spain; and [‡]Instituto de Medicina Molecular, Faculdade de Medicina, Universidade de Lisboa, Lisbon, Portugal

ABSTRACT BP100 (KKLFKKILKYL-NH_2) is a short cecropin A-melittin hybrid peptide, obtained through a combinatorial chemistry approach, which is highly effective in inhibiting both the in vitro and in vivo growth of economically important plant pathogenic Gram-negatives. The intrinsic Tyr fluorescence of BP100 was taken advantage of to study the peptide's binding affinity and damaging effect on phospholipid bilayers modeling the bacterial and mammalian cytoplasmic membranes. In vitro cytotoxic effects of this peptide were also studied on mammalian fibroblast cells. Results show a stronger selectivity of BP100 toward anionic bacterial membrane models as indicated by the high obtained partition constants, one order of magnitude greater than for the neutral mammalian membrane models. For the anionic systems, membrane saturation was observed at high peptide/lipid ratios and found to be related with BP100-induced vesicle permeabilization, membrane electroneutrality, and vesicle aggregation. Occurrence of BP100 translocation was unequivocally detected at both high and low peptide/lipid ratios using a novel and extremely simple method. Moreover, cytotoxicity against mammalian models was reached at a concentration considerably higher than the minimum inhibitory concentration. Our findings unravel the relationships among the closely coupled processes of charge neutralization, permeabilization, and translocation in the mechanism of action of antimicrobial peptides.

INTRODUCTION

Antimicrobial peptides (AMPs) form an essential part of the innate immune system of virtually all forms of life (1–7). During the last decades, AMPs have been widely studied, as they may become an alternative to conventional antibiotics, especially for the treatment of drug-resistant infections (8, 9). Hundreds of AMPs have been isolated (see a comprehensive list at http://www.bbcm.univ.trieste.it/~tossi/pag1.htm) and several thousands have been de novo designed and synthetically produced. They display a wide range of biological activities against bacteria, fungi, protozoa, enveloped viruses, and even tumor cells (9–14). Interestingly, they retain activity against antibiotic-resistant strains and do not readily elicit resistance (15–17).

Despite displaying extensive sequence heterogeneity, most AMPs share two functionally important features: a net positive charge and the ability to assume an amphipathic structure. These structural characteristics are essential for the mode of action of most AMPs, which target the microbial membrane. The net positive charge promotes their binding to the anionic microbial surface, while the amphipathic structure favors peptide insertion into the membrane (10–12,15,16,18–20). Despite extensive studies, the precise mechanism of peptide-membrane interaction and cell killing has not been firmly established for many AMPs. Several models have been proposed to account for the morphological changes involved in AMPs-mediated membrane disruption, such as pore formation (21), cell lysis (22), or peptide translocation into the cytoplasm (23). Recently, some studies have shown that, apart from membrane damage, other mechanisms may be involved including intracellular targets (9,15,16). However, in such mechanisms, peptides still must traverse the cell membrane to reach their site of action, which stresses the relevance of peptide-membrane interactions for AMP activity.

Cecropins, first isolated from the hemolymph of the giant silk moth *Hyalophora cecropia*, are some of the best studied AMPs (24–26). They represent a family of peptides composed of 31–39 amino acids with antibacterial activity against both Gram-negative and Gram-positive bacteria. Cecropins do not exhibit cytotoxic effects against human erythrocytes and other eukaryotic cells, but are susceptible to protease degradation (24,27,28). In an effort to overcome the high production costs of such long peptides and to improve their biological properties, short peptide analogs have been designed and synthesized. These studies have led to the identification of nontoxic and more stable peptide sequences displaying a broader and higher activity than their natural counterparts (29–36). In particular, the undecapeptide WKLFKKILKVL-NH_2 (Pep3), derived from the well-known cecropin A(1–7)-melittin(2–9) hybrid (30,33,34), has been found to be sufficient for antifungal and antibacterial activities, while displaying low cytotoxicity (32,37–40).

Recently, we have identified cecropin A-melittin hybrid undecapeptides derived from Pep3 which inhibit in vitro growth of economically important plant pathogenic bacteria such as *Erwinia amylovora*, *Pseudomonas syringae*

Submitted August 22, 2008, and accepted for publication November 17, 2008.

*Correspondence: macastanho@fm.ul.pt

Rafael Ferre and Manuel N. Melo contributed equally to this work.

Editor: Huey W. Huang.

0006-3495/09/03/1815/13 $2.00

doi: 10.1016/j.bpj.2008.11.053

pv. *syringae*, and *Xanthomonas axonopodis* pv. *vesicatoria* (38–40). In particular, KKLFKKILKYL-NH_2 (BP100), obtained through a combinatorial chemistry approach, displays a bactericidal effect against these bacteria as well as minimized cytotoxicity and low susceptibility to proteinase K degradation (38). Moreover, BP100 is highly effective to prevent infections of *E. amylovora* in pear and apple flowers, being only slightly less potent than streptomycin, which is the most active compound currently used in fire blight control (38).

Although it has been proposed that the mode of action of cecropins and melittin depends on the peptide concentration and membrane composition (41–45), the mechanisms involved in the action of cecropin-melittin hybrid peptides, and especially that of short undecapeptides, are very far from being completely understood. Insights into the mode of action of BP100 are essential for the full rationalization of the biological properties of this peptide as well as for their further improvement. In this study, we investigated the interaction of BP100 with different model membranes using spectroscopic methodologies, which can afford valuable information about peptide-membrane interaction. A comprehensive study was carried out to ascertain the conditions under which BP100 disrupts membranes or, alternatively, translocates across them to reach the lumen of vesicles. Moreover, the in vitro cytotoxic effects of this peptide were also studied on mammalian fibroblast cells.

MATERIALS AND METHODS

Reagents and apparatus

The ultraviolet-visible absorption and steady-state fluorescence emission assays were performed at room temperature in a model No. V-560 UV-Vis spectrophotometer (JASCO, Hachioji, Japan) and in a model No. IBH FL3-22-time-correlated single photon-counting (TCSPC) spectrofluorometer (Horiba Jobin Yvon, Longjumeau, France), equipped with a 450 W Xe lamp and double monochromators, or in a Cary Eclipse Thermo Spectronic spectrofluorometer (Varian, Palo Alto, CA), equipped with a 75 kW pulsed Xe lamp. Multiwell absorption measurements were performed in a Multiskan RC plate reader (Labsystems, Helsinki, Finland). Time-resolved fluorescence decays were collected in the FL3-22-TCSPC spectrofluorometer using a time-correlated single photon counting (TCSPC) technique with a 279-nm nanoLED source (IBH, Glasgow, UK); reduction of scattered light contribution to the decays was achieved by horizontally polarizing the excitation light with a Glan-Thompson polarizer; lifetimes were calculated from time-resolved fluorescence intensity decays using at least 10 K counts in the peak channel; fluorescence intensity decay curves were deconvoluted with the software package DAS 6.1 from IBH.

Dynamic light scattering and ζ-potential measurements were taken in a Zetasizer Nano-ZS (Malvern Instruments, Worcestershire, UK), equipped with a 633-nm HeNe laser.

We used 2-(4-(2-hydroxyethyl)-1-piperazinyl)-ethanesulfonic acid (HEPES), sodium chloride, chloroform, ethanol (spectroscopic grade), acrylamide, dimethyl sulfoxide, and trypan blue (Merck, Darmstadt, Germany). Phospholipids 1-palmitoyl-2-oleoyl-*sn*-glycero-3-phosphocholine (POPC) and 1-palmitoyl-2-oleoyl-*sn*-glycero-3-(phosphor-rac-(1-glycerol)) (POPG) were from Avanti Polar Lipids (Alabaster, AL). Cholesterol, cell culture media, serum, antimicrobials, trypsin/versine, 3-(4,5-dimethylthiazol-2-yl)-2,5-diphenyl-2*H*-tetrazolium bromide (MTT), and crystal violet stain were from Sigma (St. Louis, MO). Lipophilic quenchers 5- and 16-NS (5- and 16-doxylstearic acids, respectively) were from Aldrich Chemical (Milwaukee, WI).

All the 9-fluorenylmethoxycarbonyl (Fmoc)-amino acid derivatives, reagents, and solvents used in the peptide synthesis were obtained from Senn Chemicals International (Gentilly, France). Fmoc-Rink-4-methylbenzhydrylamine resin (0.64 mmol/g) was purchased from Novabiochem (Darmstadt, Germany). Trifluoroacetic acid, *N*-methyl-2-pyrrolidinone, and triisopropylsilane were from Sigma-Aldrich (Madrid, Spain). Piperidine and *N*,*N*-diisopropylethylamine were purchased from Fluka (Buchs, Switzerland). Solvents for high-performance liquid chromatography (HPLC) were obtained from J.T. Baker (Deventer, Holland).

Solutions were prepared in a 10 mM HEPES buffer at pH 7.4, containing 150 mM NaCl (the so-called physiologic ionic strength). All BP100 fluorescence measurements were recorded at an excitation wavelength of 275 nm, except for the experiments involving acrylamide in which the peptide was excited at 285 nm to minimize the relative quencher/fluorophore light absorption ratio.

Peptide synthesis

BP100 was synthesized as a C-terminal carboxamide on a Rink *p*-methylbenzhydrylamine resin by the solid-phase synthesis method using standard 9-fluorenylmethoxycarbonyl (Fmoc) chemistry (38). The peptide was purified by reverse-phase semipreparative HPLC on a 5 μm, 1.0 $\times$ 25 cm C18 Tracer column (Teknokroma, Barcelona, Spain) using a linear gradient from 10 to 60% acetonitrile in water with 0.1% trifluoroacetic acid over 50 min. The peptide was obtained with >95% HPLC purity. Electrospray ionization mass spectrometry was used to confirm peptide identity.

Preparation of model membrane vesicles

Large unilamellar vesicles (LUVs) of 100-nm diameter and multilamellar vesicles (MLVs) of different phospholipid composition were used as biological membrane models. MLVs were obtained by hydration of dried phospholipid films under vortex agitation; when required, multilamellarity was enhanced by first hydrating the films in a fraction of the final volume. LUVs were prepared by freezing-thawing and extruding MLVs, as described elsewhere (46). Sonication of vesicles, when needed, was carried out in an Ultrasound Technology UP200S power sonicator (Hielscher Ultrasonics, Teltow, Germany). Mammalian model systems included 100% POPC LUVs and 2:1 POPC/cholesterol LUVs. Bacterial model systems included 2:1 and 4:1 POPG/POPC LUVs.

Photophysical characterization of BP100 in aqueous solution

The linear dependence of the absorbance and fluorescence intensity of BP100 on its concentration was tested over the 0–140 μM range. To check whether peptide aggregation occurs in the aqueous phase, the Tyr fluorescence was quenched by sequentially adding aliquots of a 4 M acrylamide solution to a 15 μM peptide sample, while recording both the absorbance and fluorescence intensity. Quenching assays data were analyzed according to the Stern-Volmer formalism (47) and were corrected for simultaneous light absorption of fluorophore and quencher (48).

Peptide-membrane incorporation studies

The extent of the partition of BP100 to each model membrane was evaluated by titrating a 15 μM peptide solution with the corresponding LUVs suspension and recording the fluorescence emission. Samples were incubated for 10 min after each addition of lipid suspension. The molar ratio partition constants, K_p, were calculated by fitting the experimental data with Eq. 1, as described elsewhere (49). The quantities I_W and I_L are the fluorescence intensities the mixture would display if all the peptide is in the aqueous or

the lipidic phase, respectively; γ_L is the phospholipid molar volume, which is considered to be 0.763 M^{-1}, corresponding to the typical value for liquid crystalline lipid bilayers (50); and [L] is the phospholipid concentration. Fluorescence data were corrected both for dilution and scattered light (51),

$$\frac{I}{I_W} = \frac{1 + K_p\gamma_L\frac{I_L}{I_W}[L]}{1 + K_p\gamma_L[L]}, \quad (1)$$

$$K_p = \frac{[BP100]_L}{[BP100]_W}, \quad (2)$$

where $[BP100]_L$ and $[BP100]_W$ are the peptide concentrations in the lipid volume or in the aqueous phase, respectively. It should be noted that because K_p implicitly includes electrostatic contributions that may be dependent upon the global peptide concentration, it should be taken as an apparent partition constant (52).

Membrane saturation studies were carried out with 2:1 POPG/POPC LUVs. Saturation points were determined by adding small aliquots of a 750 μM stock peptide solution to an LUV suspension (phospholipid concentrations of 0, 40, 75, 125, 175, and 250 μM) containing 100 mM acrylamide. The fluorescence emission was recorded after 10 min of each peptide addition. To prevent dilution of acrylamide, the stock peptide solution also contained 100 mM of this aqueous phase quencher. The peptide/lipid (P/L) ratio at saturation (σ) and K_p were calculated by fitting the obtained saturation points with Eq. 3, as described elsewhere (53):

$$[P] = \frac{\sigma}{K_p\gamma_L} + \sigma[L]. \quad (3)$$

In-depth membrane localization studies

Differential quenching studies were carried out by sequentially adding aliquots of a lipophilic quencher—either 5-NS or 16-NS—to a LUV suspension previously equilibrated with 10 μM BP100; two different LUV concentrations—125 and 250 μM—were used so as to set either saturation or nonsaturation states and quencher concentration was increased or reduced accordingly; time-resolved fluorescence measurements of the Tyr in BP100 were taken. To prevent bilayer alterations while adding the 5- and 16-NS quencher aliquots, prepared in ethanol, care was taken to keep final ethanol concentrations below 2% (v/v) (54). Results were analyzed with a methodology based on the knowledge of the quenchers' in-depth distributions in the membrane (55), modified to implement a least-squares fitting to the data.

Vesicle permeabilization studies

The kinetics of BP100-induced vesicle leakage was monitored by Co^{2+} quenching of the fluorescence of 1% N-NBD-PE (56) incorporated into 125 μM 2:1 POPG/POPC vesicles, at BP100 concentrations ranging from 0 to 25 μM. Briefly, experiments were carried out by adding aliquots of BP100 to a suspension of vesicles in the presence of 20 mM $CoCl_2$. The $CoCl_2$, which is unable to permeate phospholipid membranes, was added to the vesicles shortly before the measurement, quenching the outer leaflet N-NBD-PE fluorescence. The kinetics were started with the addition of BP100. Permeabilization of the membrane to the Co^{2+} ions results in further quenching of the inner leaflet N-NBD-PE population. The decrease of NBD fluorescence emission intensity at 515 nm was monitored with excitation at 460 nm. The percentage of leakage at time t after peptide addition was determined from Eqs. 4–6,

$$\%\ \text{leakage}\ (t) = \left[Co^{2+}\right]_{in}(t)/\left[Co^{2+}\right]_{out}(t) \approx [Co^{2+}]_{in}(t)/[Co^{2+}]_{TOTAL,} \quad (4)$$

where $[Co^{2+}]_{TOTAL}$, $[Co^{2+}]_{in}$, and $[Co^{2+}]_{out}$ correspond to the global, luminal, and external quencher concentrations, respectively. The approximation of $[Co^{2+}]_{out}(t)$ as $[Co^{2+}]_{TOTAL}$ can be made because no significant decrease of external quencher concentration is expected upon leakage: at these lipid concentrations, the total internal vesicle volume can be calculated to be <0.005% of the sample volume (57). From the collisional quenching Stern-Volmer formulation (58), quencher concentrations can be related with fluorescence intensities,

$$\%\,\text{leakage}\,(t) = \frac{-\Delta I_{in}(t)}{I_{in}(t) \times K_{SV}} \div \frac{-\Delta I_{max}}{I_c \times K_{SV}} = \frac{I_c \times \Delta I_{in}(t)}{I_{in}(t) \times \Delta I_{max}} \quad (5)$$

where K_{SV} is the Stern-Volmer quenching constant, I_{in} is the contribution of inner leaflet fluorophores to the global fluorescence intensity, ΔI_{in} is the change in I_{in} after peptide addition, ΔI_{max} is the maximum change in global fluorescence from before quencher addition to complete leakage, and I_c corresponds to the minimum fluorescence intensity at 100% leakage, obtained by vesicle sonication. There are two populations contributing to the global fluorescence: the inner and outer leaflet fluorophores; because the external quencher concentration remains virtually constant, the fluorescence intensity of the outer fluorophore fraction will also be approximately constant and $\Delta I = \Delta I_{in}$, where ΔI is the change in global intensity upon peptide addition. In addition, from the moment of quencher addition, the external fraction decreases to its minimum possible fluorescence intensity which, given the large size of a vesicle, is roughly one-half of I_c. This allows the substitution of $I_{in}(t)$ as $I(t) - 0.5 \times I_c$,

$$\%\ \text{leakage}\ (t) = \frac{I_c \times \Delta I(t)}{\left(I(t) - 0.5I_c\right) \times \left(I_c - I_{pre}\right)}, \quad (6)$$

where I_{pre} is the global fluorescence intensity before quencher addition.

Leakage kinetics were tentatively fitted with the system of ordinary differential equations described in Gregory et al. (59).

Membrane translocation studies

To determine the occurrence and extent of peptide translocation across the membrane a novel method was devised: the increase of BP100 fluorescence upon membrane interaction was followed after MLV addition. A control experiment was performed in which the interaction kinetic was instead initiated with LUVs produced from the same suspension of MLVs. In the occurrence of translocation, the interaction kinetic with the MLVs would be slowed down with respect to LUV interaction due to the multiple membrane crossing steps. In the absence of translocation, although the lipid concentration is the same in MLV and LUV suspensions, the peptide would sense an apparently lower concentration of lipid in an MLV suspension, as only the outer lipid shell is accessible; as such, fluorescence would never increase as much with MLVs as with LUVs (see Fig. 1 for details). A quantity of 40 μM 2:1 POPG/POPC LUVs and MLVs were used. The sensitivity in the detection of peptide-lipid interaction was improved by adding aliquots of 200 mM of acrylamide to increase the fluorescence change upon binding. Potential artifactual increases of BP100 emission due to scattered light contribution were controlled by monitoring the ratio of fluorescence intensities at 303 and 330 nm.

Vesicle aggregation and charge studies

Turbidity studies were carried out by monitoring the changes induced by BP100 in the optical density (OD) of a vesicle suspension. Briefly, aliquots of a 1 mM BP100 stock solution were added to 125 μM 2:1 POPG/POPC vesicle suspensions. Peptide concentrations tested ranged from 0 to 21 μM. The OD was recorded at 450 nm every 2 s for 30 min after peptide addition.

Dynamic light scattering measurements were carried out in similar conditions as the OD measurements. BP100 concentrations ranged from 0 to 16.5 μM. The ζ-potential measurements were performed at 250 μM lipid and at BP100 concentrations up to membrane saturation.

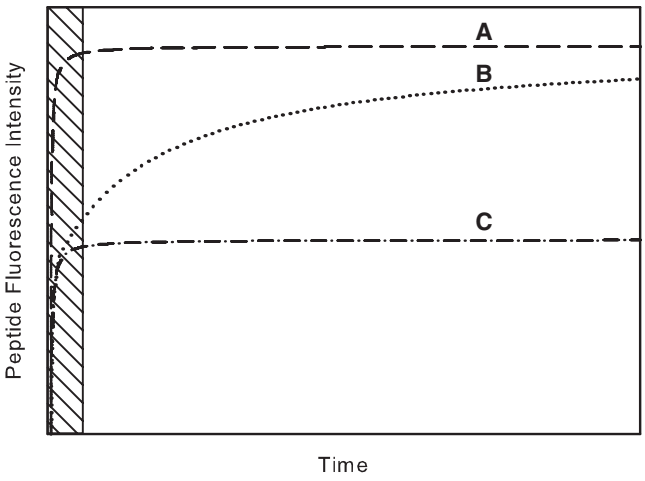

FIGURE 1 Expected fluorescence increase kinetics of BP100 in interaction with LUVs or MLVs. (*A*) LUVs with or without the occurrence of translocation: the entire lipid is accessible to the peptide at time 0 resulting in a fast interaction kinetics. (*B*) MLVs, with peptide translocation: at time 0, only a fraction of the lipid is accessible to the peptide, resulting in a fast, but partial, increase in fluorescence; as the peptide translocates, more lipid becomes accessible, and a full fluorescence increase is eventually reached at a lower rate. (*C*) MLVs, without translocation: there is a fast interaction with the accessible fraction of lipid, but no subsequent increase is expected, as no more lipid becomes accessible. The hatched region indicates the approximate relative measurement dead time for BP100 under our setup.

Cytotoxicity assays

Cell culture

V79 Chinese hamster lung fibroblast cells (MZ subline (60)) were used for the cytotoxicity assays (61). They were routinely cultured in 175 cm^2 tissue flasks in Ham's F-10 medium, supplemented with 10% newborn calf serum and 1% penicillin/streptomycin, in a humidified incubator at 37°C with 5% CO_2. Cells were routinely subcultured in the semiconfluent state over a maximum of eight passages and regularly tested negative for *Mycoplasma*. The V79 cells used in this study were kindly obtained from Prof. H. Glatt (German Institute of Human Nutrition, Germany) and were routinely maintained and kindly provided by Dr. Nuno Oliveira (University of Lisbon, Portugal).

Exposure conditions in the assays

V79 cells were suspended in 180 μL culture medium in 96-well plates, at a density of 5×10^3 cells/well, optimized to keep the cultures in optimal growth during the whole experiment. After seeding, the plates were incubated for 24 h before the experiment. BP100 was dissolved in HEPES and added to 20 μL of the medium to obtain final concentrations of 90, 60, 40, 30, and 10 μM. Two replicates for each peptide concentration were used. Each plate contained a negative control (culture medium + 10% HEPES) and a positive control (culture medium + 10 mM H_2O_2). Cell viability was measured after incubation for 24 h at 37°C with 5% CO_2.

Cell viability assays

Three assays were performed to test the cell viability. The MTT assay was used to investigate the effect of BP100 on the mitochondrial dehydrogenase activity, measured as the ability of viable cells to produce formazan crystals (62). The cells were rinsed once with phosphate-buffered saline and then 200 μL MTT solution (5 mg/ml) were added to each well. After 2.5 h incubation at 37°C, 200 μL dimethyl sulfoxide were added to each well to dissolve the purple formazan crystals (63). The absorbance of the resulting dispersion was determined at 595 nm in the multiwell scanning spectrophotometer.

Crystal violet is a dye that accumulates in the cell nucleus and was applied in this study as an indicator for cell viability (62). The fixed dye correlates directly with the nuclear DNA content, and thus also with the cell number. After its application, nonviable, nonadherent cells were washed. The fixed crystal violet was solubilized in 10% SDS for 20 min and the OD of the solution was measured at 595 nm.

The ability of cells to stain with trypan blue was used to investigate the loss of plasma membrane integrity (64). The cells were washed with phosphate-buffered saline, dispersed with 40 μL trypsin EDTA and the resulting cell suspension was diluted in 10 μL of culture medium. 20 μL of the mixed cell suspension were added to 20 μL of 0.4% trypan blue fresh solution, prepared in NaCl 0.9%, to stain nonviable cells. Cell viability was expressed as the percentage of unstained cells (65).

Statistical analysis and regression modeling

To account for the interplate variability, the absolute values of the cell viable parameters were normalized to the average of the negative controls (100% viability) and the positive controls (0% viability, corresponding to 100% cell death) (64). Statistical concentration-response analyses were performed in the same way for all three in vitro tests by fitting a three-parameter nonlinear regression Logit model to the data (66). Dunnett's test (α = 5%) was employed to determine statistical significant differences between the treated groups and the negative controls. IC_{50} values were determined as the midpoint of the fitted curves.

RESULTS

Photophysical characterization in aqueous solution

Both the absorbance and fluorescence intensities of BP100 depended linearly on concentrations up to 140 μM (data not shown). The obtained photophysical parameters were similar to those of free Tyr: the excitation maximum for BP100 was at 275 nm (λ_{em} = 306 nm), which is coincident with the wavelength of maximal electronic absorption. The calculated absorptivity coefficient (ε) at this wavelength was 1.40×10^3 M^{-1} cm^{-1}. The quenching of BP100 by acrylamide followed a linear Stern-Volmer relationship up to 250 mM of quencher, with a K_{SV} of 15.1 M^{-1} (not shown).

Membrane insertion studies

For all the membrane models tested, an increase of fluorescence intensity was observed upon the partition of BP100 between the aqueous buffered phase and the lipidic membrane studied (Fig. 2). Partition parameters are summarized in Table 1.

For the neutral systems, liquid-crystal POPC and liquid-ordered 2:1 POPC-cholesterol LUVs, the increase of fluorescence followed a hyperbolic-like relationship (Fig. 2 *A*). In contrast, the anionic systems 2:1 POPG/POPC and 4:1 POPG/POPC deviated from this behavior (Fig. 2 *B*). At low lipid concentrations, an overshoot of the fluorescence intensity was detected. This result was assigned to reflect membrane saturation. To confirm this hypothesis, membrane saturation studies were carried out for the 2:1 POPG/POPC system (Fig. 3). Saturation points were identified from the

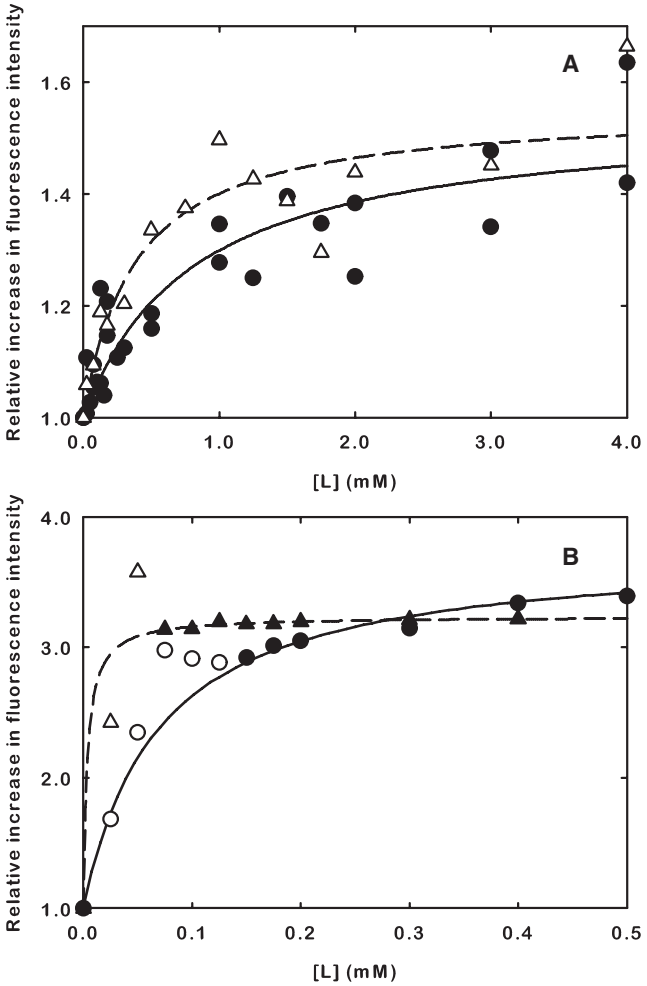

FIGURE 2 Lipid titrations of 15 μM BP100 with different LUV systems. Lines represent the fitting parameters of the data to the partition model in Eq. 1. (*A*) POPC (•, *solid line*) and 2:1 POPC/cholesterol (△, *dashed line*) LUVs. (*B*) 4:1 POPG/POPC (•, *solid line*) and 2:1 POPG/POPC (▲, *dashed line*) LUVs; deviations occurred at low lipid concentrations and those data points (*empty*) were removed from the fittings. The difference in the required amounts of lipid for the titrations in panels *A* and *B* indicates a much higher partition toward the anionic models; this is confirmed by the obtained partition constants. Fit parameters are summarized in Table 1.

breaks observed in the curves obtained from titration of vesicles with BP100 and were fitted with Eq. 3 (Fig. 3, *inset*). A K_p value of 8.41×10^4 was obtained and a σ of 0.118 was determined, which corresponds to 8.4 phospholipids per peptide at the saturation of the vesicles.

The depth of membrane internalization was probed using stearic acid molecules labeled at different carbon positions (carbons 5 and 16 for 5- and 16-NS, respectively) with tyrosine quenching nitroxyl groups. With previous knowledge of the in-depth distribution of each quencher, an integrated approach was used to infer the distribution of the tyrosine residue of the peptide from each quencher's quenching profile (based on (55)). These profiles did not change significantly upon saturation (not shown), indicating little change in the in-depth localization of the peptide. This was confirmed after analysis: in the absence of saturation, the average in-depth localization from the bilayer center was 10.5 Å and the distribution half-width at half maximum was 3.2 Å (a Lorentzian distribution was assumed); under saturation, these parameters were 11.2 Å and 2.4 Å, respectively.

TABLE 1 Summary of the characteristics of each studied system: constitution and partition parameters determined using Eq. 1

Modeled system	Constituent phospholipids	$K_p/10^3$	I_L/I_W
Bacterial membrane models			
Outer leaflet	2:1 POPG/POPC	30.8 ± 6.2	3.59 ± 0.06
Inner leaflet	4:1 POPG/POPC	87.6 ± 9.8	3.58 ± 0.02
Mammalian membrane models			
Outer leaflet	100% POPC	1.6 ± 0.5	1.54 ± 0.06
Outer leaflet + cholesterol	2:1 POPC/cholesterol	3.5 ± 1.3	1.55 ± 0.06

Vesicle permeabilization studies

Fig. 4 displays the leakage kinetics induced by increasing BP100 concentrations. BP100 induced vesicle leakage in a dose-dependent manner. It should be noticed that from 15 μM peptide the kinetics display a markedly sigmoidal rise; this is evident in Fig. 4. A transition at 15 μM of BP100 is also clearly observed in the leakage percentage at 390 s (Fig. 4, *inset*). Thus, for 125 μM lipid, 15 μM is a critical BP100 concentration dictating the transition between two different regimes of peptide-lipid interactions.

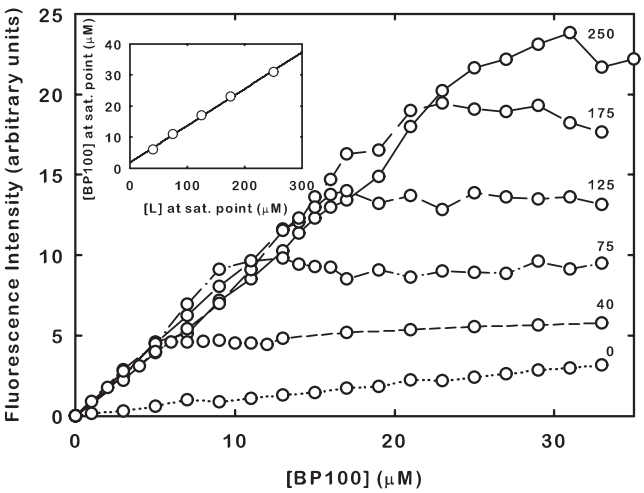

FIGURE 3 Titration of several concentrations of 2:1 POPG/POPC LUVs with BP100 in the presence of 100 mM acrylamide (lipid concentration is indicated in μM for each set of points). Saturation points were identified from the breaks in each curve. (*Inset*) Linear dependence of the global peptide and lipid concentrations at the saturation points, fitted according to Eq. 3, yielding a saturation proportion of 8.4 phospholipids per peptide and a partition constant of 8.41×10^4.

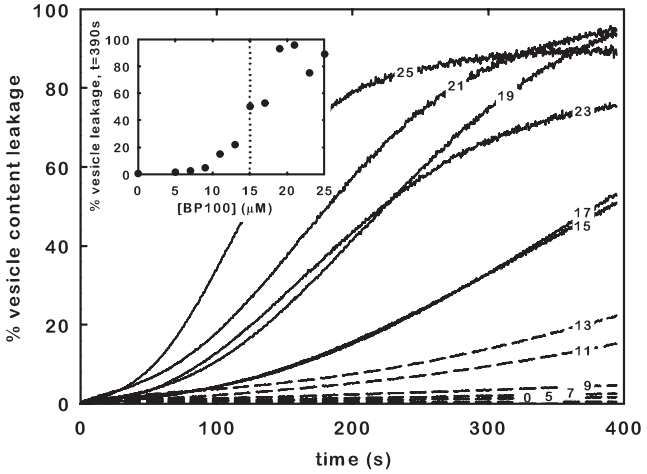

FIGURE 4 Time course of BP100-induced vesicle leakage to Co^{2+} with 125 μM 2:1 POPG/POPC LUVs doped with 1% N-NBD-PE; each curve corresponds to a different BP100 concentration, indicated in the figure in μM. Dashed lines correspond to subsaturation conditions. (*Inset*) Leakage percentage at 390 s in which a transition in behavior with BP100 concentration is evident; this transition occurs close to the expected membrane saturation point for the used lipid concentration, indicated by the dotted line.

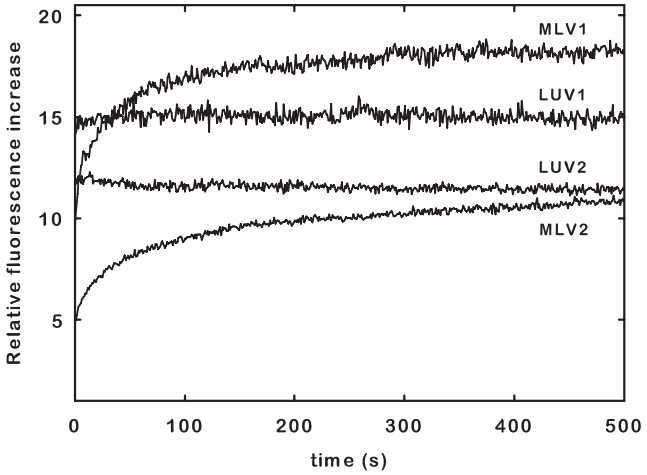

FIGURE 5 Time course of BP100 interaction with 40 μM 2:1 POPG/POPC LUVs and MLVs. LUV1 and MLV1: 4 μM BP100. LUV2 and MLV2: 12 μM BP100. Chosen BP100 concentrations are below and above membrane saturation, as per Eq. 3. Comparison with the expected kinetic profiles (Fig. 1) indicates the occurrence of peptide translocation in both cases.

The sigmoidal curves could be fitted with the model described by Gregory et al. (59) (not shown), even though in their work only hyperbolic-like kinetics were fit. Both rate constants of pore formation/dissipation needed to be two-to-three orders-of-magnitude lower than those observed by Gregory et al. (59) to generate a sigmoidal behavior comparable to the one observed in Fig. 4. Further quantitative analysis of leakage parameters is, however, not reliable, due to multiple minima in the solution space and some degree of correlation.

Membrane translocation studies

There were marked differences between the peptide-MLV and peptide-LUV interaction kinetics (Fig. 5). Whereas the increase in peptide fluorescence intensity upon LUV addition was almost instantaneous, the MLV-induced increase spanned several minutes. Fluorescence intensity for the MLV additions started out lower than that induced by LUV additions of the same lipid concentration, but rose to approximately the same relative level, as expected for the occurrence of translocation (Fig. 1). To better compare the fluorescence change at both peptide concentrations, Fig. 5 depicts the relative increase in fluorescence upon lipid addition. As a consequence there are small differences in the endpoint of the kinetics at low BP100 concentrations (Fig. 5—MLV1 and LUV1), attributable to error introduced by the low initial Tyr fluorescence signal and further aggravated by the use of acrylamide.

Vesicle aggregation and surface charge studies

Apart from a transient initial increase in turbidity, no significant changes in vesicle OD were observed at peptide concentrations <15 μM (Fig. 6). For peptide concentrations at or >15 μM, however, there was a remarkable time-dependent increase of the OD due to liposome aggregation induced by BP100 (Fig. 6, *inset*).

A related change was also observed with light scattering measurements where the average particle diameter of the LUV suspension increased by ~10-fold (Fig. 7). Similarly to permeabilization, the BP100-induced increase of vesicle turbidity/aggregation displays a transition between two regimes close to 15 μM, with 125 μM of lipid.

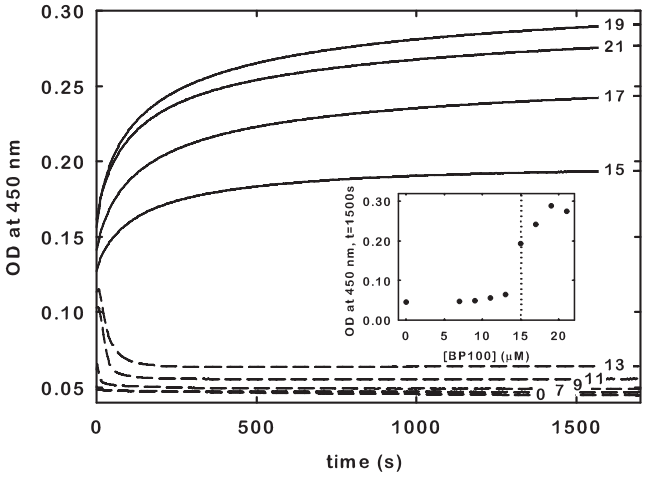

FIGURE 6 Time course of BP100-induced OD change (λ = 450 nm) of 125 μM 2:1 POPG/POPC LUVs; each curve corresponds to a different BP100 concentration, indicated in the figure in μM. Two different kinetic behaviors are evident. Dashed lines correspond to subsaturation conditions. (*Inset*) OD_{450} at 1500 s. The transition in behavior is evident above 15 μM; as with vesicle leakage (Fig. 4), this transition occurs close to the expected membrane saturation point for the used lipid concentration, indicated by the dotted line.

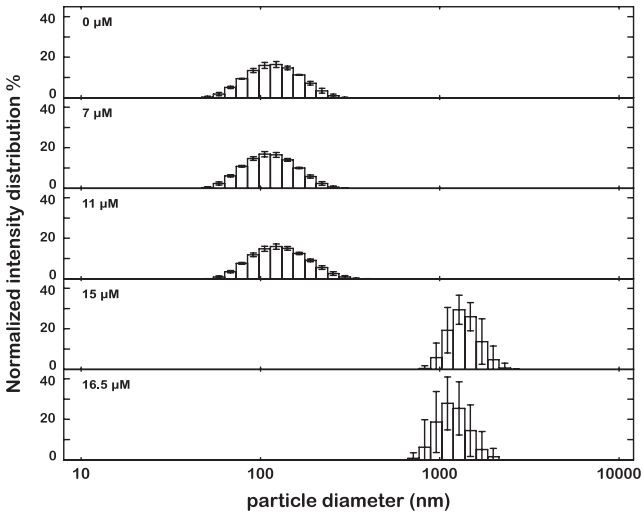

FIGURE 7 Normalized intensity distribution determined by dynamic light scattering of the particle sizes of a 125 μM 2:1 POPG/POPC LUV suspension in the presence of increasing BP100 concentrations (*error bars* represent SD). Above membrane saturation, which is expected at ~15 μM BP100 at this lipid concentration, a significant increase in particle size and heterogeneity is observed, in agreement with the occurrence of vesicle aggregation. This result correlates with the observed distinct behavior of BP100-induced OD change below and above saturation (Fig. 6).

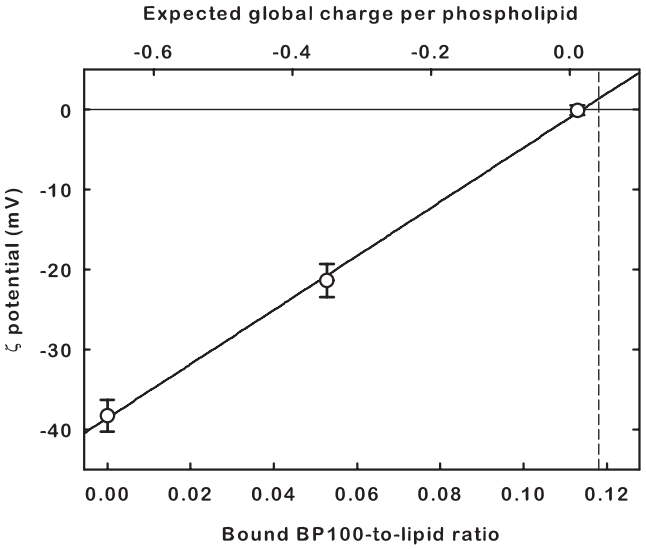

FIGURE 8 The ζ-potential of 250 μM 2:1 POPG/POPC LUV in the presence of different BP100 concentrations (*error bars* represent SD). Peptide concentrations are displayed either as bound peptide/lipid ratios (calculated with the partition constant obtained from Eq. 3) or as the estimated global charge per phospholipid assuming a 6^+ charge on the peptide. A linear regression of the points is displayed as a guide to the eye. The saturation ratio is indicated by the dashed line. A neutralization of the LUV charge at the saturation point was observed, in agreement with what was expected from the saturation proportion (Fig. 3), the peptide charge, and the composition of the system.

The particles' ζ-potential was -38.3 mV in the absence of peptide but was brought close to zero (-0.1 mV) at saturation (Fig. 8); aggregation and increase in turbidity prevented ζ-potential measurement at higher peptide concentrations.

Effects of BP100 exposure on cell viability

Fig. 9 depicts the effects of BP100 on the mitochondrial activity, cell monolayer adherence, and membrane integrity of cultured hamster fibroblasts. All cell viability parameters responded to the peptide (10–90 μM) in a clear dose-dependent way. At the highest tested concentration (90 μM), low cell viability (<10%) was observed. The peptide concentrations, at which 50% inhibition was expected (IC_{50}), were interpolated from the regressions for each viability assay, and ranged from 51.1 μM, for the crystal violet stain, to 64.3 μM for the trypan blue assay.

DISCUSSION

The biological activity of small, cationic antimicrobial peptides has been largely associated with their interaction with membranes. It is widely believed that for many of these peptides, membrane disruption is the primary mechanism of cell killing (10–12,15,16,18–20). However, their exact mode of action is still poorly understood. Elucidating their mechanism of action and their specific membrane damaging properties is crucial for the rational design of novel antibiotic peptides with high antibacterial activity and low cytotoxicity. With these observations in mind, and considering that BP100 contains a Tyr residue, which makes it intrinsically fluorescent, we have exploited its photophysical properties to obtain information about its binding affinity and damaging effect on bilayers having a lipid composition

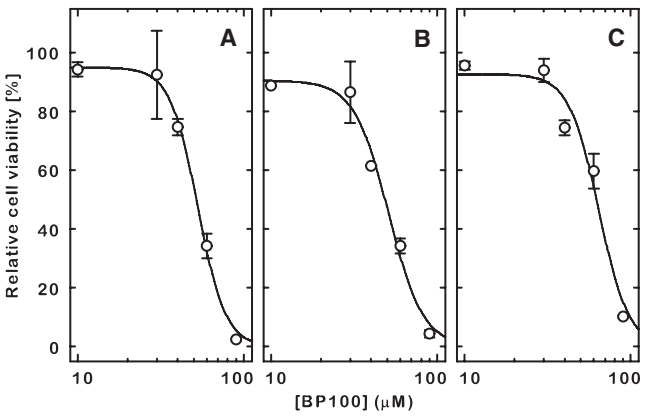

FIGURE 9 Effects of BP100 on the viability of V79 Chinese hamster lung fibroblast cells after 24 h exposure (*error bars* represent SE). (*A*) Mitochondrial activity determined by the MTT assay; $IC_{50} = 52.9$ μM. (*B*) Loss of monolayer adherence estimated by the crystal violet assay; $IC_{50} = 51.1$ μM. (*C*) Plasma membrane integrity estimated by the trypan blue assay; $IC_{50} = 64.3$ μM. Logit curves were fitted to the data and are shown as lines. The IC_{50} values are proportionally greater-than the MIC, by approximately the same factor as the partition constants toward the anionic bacterial models are greater-than toward the neutral mammalian models, suggesting a concentration-dependent disruption mechanism.

similar to that of the bacterial and mammalian cytoplasmic membranes.

Photophysical characterization of BP100 in aqueous solution

The photophysical characterization of peptides in aqueous solution is a prerequisite to understand their interaction with phospholipid model membranes. The observed behavior of BP100 in aqueous solution reflects that peptide aggregation does not occur at the studied peptide concentration range. This is supported by the linear dependencies of fluorescence emission intensity and electronic absorption on concentration and by the obtained λ_{exc}, λ_{em}, and ε-values as they are similar to those of free Tyr (275, 303, and 1400, respectively (47)), indicating that the Tyr in BP100 is exposed to an aqueous environment (47). Moreover, a linear Stern-Volmer plot for the fluorescence quenching of BP100 with acrylamide is observed up to 250 mM (not shown). In addition, there are no significant differences between the obtained K_{SV} and the one for acrylamide quenching of free Tyr, evidencing that Tyr is totally accessible to the aqueous phase. The absence of aggregation observed for BP100, together with its overall positive charge (+6), could account for its high solubility in aqueous solution and facilitates the interpretation of the peptide-membrane interaction results.

Membrane insertion studies

The extent of the partition of BP100 into model membranes was studied using a partition model described by Santos et al. that allows the calculation of the Nernst partition constant (K_p) from fluorescence intensity (I) versus phospholipid concentration ([L]) plots at a constant peptide concentration ([P]) (49). The K_p, defined as the ratio between the equilibrium membrane-bound and aqueous phase peptide concentrations, provides an easy assessment of the extent of peptide-membrane interaction (Eq. 2). For both neutral systems POPC and 2:1 POPC/cholesterol LUVs, used as models of the outer leaflet of mammalian membranes, the fluorescence intensity increased following an hyperbolic-like relationship (Fig. 2 *A*). The moderate K_p values obtained for vesicles composed of 100% POPC and POPC/cholesterol mixtures (Table 1) could be attributed to the hydrophobic effect and the van der Waals forces that are likely to dominate the interactions between the neutral lipids and the hydrophobic residues of BP100. In this case, no specific interaction with cholesterol was observed, which is an indicator of low toxicity toward mammalian cells. Furthermore, cholesterol seems to play an important role in preventing the intercalation of AMPs into eukaryotic cell membranes (67); its presence and the absence of acidic phospholipids in the eukaryotic membranes could account for the low cytotoxicity displayed by BP100 against erythrocytes (38).

For the anionic liquid-crystalline 2:1 and 4:1 POPG/POPC vesicles, which served as models for bacterial cell membranes, the partition curves deviated from the hyperbolic-like progression at low lipid concentrations (Fig. 2 *B*). A similar behavior has been recently reported for the antimicrobial peptide omiganan and has been attributed to a membrane saturation process: at low phospholipid concentrations, membrane saturation may occur when the bound peptide concentration, hypothetically dictated by K_p, is higher than what the membrane can accommodate (53); under these conditions, interaction changes may occur, as has also been described for other AMPs upon the crossing of threshold P/L ratios (68,69). Since the model of Santos et al. (49) is not well suited to study these saturated systems, the K_p values were obtained by fitting only the nonsaturated points to the partition model (Fig. 2 *B* and Table 1). This approach is obviously subject to error because the initial points of the curve, which are important for the accurate calculation of K_p, cannot be used. However, even with great associated errors, the obtained partition constants were one or more orders-of-magnitude higher than those of the neutral systems (Table 1). These results are consistent with the expected preference of cationic peptides for negatively charged membranes as a consequence of the strong electrostatic interaction.

To ensure that the deviation observed in the partition curves of the anionic vesicles was due to a saturation of the system, membrane saturation studies were carried out using 2:1 POPG/POPC LUVs. LUV suspensions were titrated with peptide in the presence of acrylamide while monitoring BP100's fluorescence intensity. Acrylamide is an aqueous quencher that facilitates the identification of alterations in the phase localization of peptides. In a nonsaturation regime, a linear increase of the fluorescence intensity is expected: as per the formalism behind Eq. 1, the fractions of the peptide in each phase are constant with constant [L]; therefore, any variation in peptide concentration will result in a proportional increase in each of these fractions and, also therefore, in a global proportional increase of the fluorescence intensity (53). Conversely, if saturation occurs, the membrane will not be able to accommodate any more peptide, which will then remain in the aqueous phase. Because acrylamide quenches preferentially the fluorescence of the aqueous phase peptide population, a weaker progression of the fluorescence intensity, relatively to a nonsaturation state, should then be detected (53). This behavior was indeed observed in the BP100 titrations (Fig. 3), showing the occurrence of saturation: two different slopes were obtained for each I versus [P] curve. The first slope corresponds to a nonsaturated state while the second one, which is similar to that of the curve in the absence of lipid, can be ascribed to a saturation of the system. The saturation points could be easily obtained from the breaks of the initial slopes of each titration curve. It was observed that the I versus [P] curve with [L] = 125 μM had its saturation point close to [P] = 17 μM (Fig. 3), which is slightly higher than the peptide concentration that yielded an I versus [L] curve

with a deviation maximum close to [L] = 125 μM (Fig. 2 *B*). This result supports the hypothesis that the deviations observed in the partition curves correspond to a saturation of the membrane.

Further information from the saturation phenomenon was obtained by representing the saturation point ([P],[L]) pairs for the 2:1 POPG/POPC LUVs (Fig. 3, *inset*). This system followed Eq. 3, which defines the total amount of peptide at which a saturation point occurs as a linear function of the amount of lipid in the system, and allows the calculation of σ—the P/L ratio at saturation—and the Nernst partition constant K_p. However, it should be noticed that the values for K_p have large associated errors because they are calculated from the reciprocal of a small intercept. Despite that, the obtained K_p (8.41×10^4) had the same order of magnitude as that determined from the partition curve using the model of Santos et al. (49) (3.08×10^4). In addition, the saturation P/L ratio was 0.118, which corresponds to 8.4 phospholipids per peptide directly in contact with the membrane at the saturation. Because there are 2/3 anionic phospholipids in the used system, there will be 5.6 negatively charged phospholipids per peptide at saturation. Interestingly, this number is very close to the expected charge of the peptide (+6) at pH 7.4, which suggests that electroneutrality is reached at the saturation of the system.

There was no significant alteration in the tyrosine in-depth location upon saturation, indicating that most of BP100 molecules maintain their positioning within the membrane. The location of the tyrosine residue, approximately halfway across the membrane leaflet, is coherent with a relatively deep burying of the peptide if it adopts, as expected (40), a horizontally oriented α-helical structure. The lysines have the ability to snorkel and keep their charged amino groups near the headgroup region (70,71) while the hydrophobic side chains could go as far as the bilayer center. This localization within the bilayer is likely responsible, at least in part, for the membrane destabilizing capabilities of BP100.

Vesicle permeabilization studies

Investigations on the mode of action of AMPs, such as cecropins and melittin, have shown that they exert their activity by inducing the formation of transmembrane pores or by causing cell lysis, depending on both the peptide concentration and the membrane composition (41–45). Moreover, it has been reported that cecropin-melittin hybrids are also able to cause membrane permeabilization (72,73). These findings prompted us to test BP100-induced permeabilization of model lipidic membranes.

Results showed that BP100 has an important permeabilizing effect dependant on peptide concentration. The increase in the permeabilization rate with BP100 concentration is, however, not linear (Fig. 4). The clear change of behavior at ~15 μM peptide, toward faster, sigmoidal, and more intense leakage kinetics—visible both in the permeabilization kinetics (Fig. 4) and in the leakage percentage profile at 390 s (Fig. 4, *inset*)—occurs very close to the peptide concentration expected to cause membrane saturation for the 125 μM lipid concentration (Fig. 3). These results show that membrane saturation affects more than just the amount of bound peptide: high P/L ratios at, or close to, membrane saturation are able to induce a change in a functional property of the peptide. The sigmoidal leakage kinetic induced by BP100 is uncommon, as such profiles are usually hyperbolic-like (74). Nevertheless, a similar kinetic was recently observed for an unrelated AMP (74). In both these cases, because the interaction with LUVs is not a limiting step (Fig. 5, LUV *traces*), the lag involved in the sigmoidal behavior may be related to postbinding events in the membrane (74).

Further information was extracted by fitting the data with the model used by Gregory et al. (59) to describe cecropin A-induced leakage. This model was only used to fit hyperbolic-like kinetics, but, even in those cases (59), close inspection of the model in the first seconds of each kinetics does reveal a brief sigmoidal behavior. Upon fitting, the magnitude of this behavior could only be manipulated to match the timescale of BP100-induced leakage kinetics by lowering the k_1 and k_2 constants of the model two-to-three orders of magnitude, relative to the values obtained in Gregory et al. (59). As these parameters are the rate constants of pore forming/dissipation, this result suggests that, after binding, BP100 becomes disruptive at a slower rate than cecropin A.

The high degree of peptide-induced leakage after saturation may reflect severe membrane damage or lysis, whereas the lower permeabilization before saturation could reflect a lesser destabilization of the membrane upon peptide binding. High P/L ratios close to saturation would then act as the trigger between these two states, and could be the biophysical parallel to the in vivo onset of antibacterial activity. This is supported by the fact that the threshold dependence on peptide concentration (Fig. 4, *inset*) could not be accounted for with data fitting without assuming some kind of parameter change with increasing BP100 concentration—such as an increase in the mentioned k_1 and k_2 disruption rates. Although hypothetical, this scenario is plausible, and stresses the importance of high local peptide concentrations in the membrane.

Membrane translocation studies

The determination of the occurrence of membrane translocation is an important functional characterization: a nontranslocating peptide can only exert its activity at the extracellular/membrane level, whereas one crossing a membrane may also have cytoplasmic targets. However, detection of translocation can be troublesome, and, although there are several methods available, many require peptide derivatization or have limited applicability (75).

Despite there being other published methods where MLVs are used to enhance an internalization effect (75,76), the method developed in our work is extremely simple and requires only that the peptide has intrinsic fluorescence and that its interaction kinetics with LUVs are significantly faster than its translocation kinetics; quencher enhancement is not an absolute requirement. The results clearly showed a translocation behavior at both high and low P/L ratios (Fig. 5). As predicted in Fig. 1 for a translocating peptide, the interaction with MLVs was slower than with LUVs, but eventually reached the same fluorescence increase. Occurrence of translocation is unequivocal and, together with the permeabilization assays, constitutes a further proof of the membrane activity of the peptide.

Vesicle aggregation and surface charge studies

Turbidity measurements have been described as an useful tool to investigate the affinity of cationic peptides toward charged vesicles (77). The stability of a dispersion of charged vesicles is mainly governed by three types of forces: electrostatic repulsion, van der Waals attraction, and hydration (77). Cationic peptides can alter the charge density of the vesicle surface inducing vesicle aggregation, which can be followed as an increase of the OD. Turbidity results showed two different kinetic patterns depending on BP100 concentration (Fig. 6). For 125 μM lipid (2:1 POPG/POPC LUV) and peptide concentrations <15 μM, which correspond to a nonsaturated state, no significant changes in turbidity were observed. However, when membrane saturation occurs (≥ 15 μM peptide), the optical density of the solution increased until a plateau was reached, ~30 min after the addition of BP100. This increase is likely due to vesicle aggregation induced under membrane saturation conditions. These results confirm the affinity of BP100 for acidic phospholipids and reinforce the hypothesis that electroneutrality is reached at the membrane saturation point.

These conclusions were confirmed using light scattering methodologies: the change in the LUV suspension OD is related to an increase in the average particle size from 100 nm—in the absence of peptide and up to saturation—to >1 μm upon saturation (Fig. 7). In addition, ζ-potential measurements in this range showed that BP100 brings the LUV charge to approximate electroneutrality at saturation, confirming the prediction based on the saturation proportion (Fig. 8). This effect is certainly favoring vesicle aggregation by canceling the electrostatic repulsion between them.

Partition, saturation, and prediction of MIC

During our recent investigations, we have found that minimum inhibitory concentration, MIC, and saturation can be correlated for peptides, such as omiganan (53). For this peptide, MICs were found to be similar to the peptide concentration needed to reach the saturation state, reflecting the existence of possible saturation-triggered antimicrobial mechanisms. Since findings from BP100-membrane interaction studies also suggest that membrane saturation is important for the activity of this peptide, we examined whether the results obtained are in agreement with the experimental MIC values.

As previously reported (53), under typical bacterial titers and using the MIC as the total peptide concentration, the membrane-bound peptide concentration ($[P]_L$) is given by $K_p \times$ MIC. On the other hand, σ can be determined as $[P]_L \times \gamma_L$. Combining both expressions, the MIC can be readily calculated as $\text{MIC} = \sigma/(K_p \times \gamma_L)$. Using the obtained σ (0.118) and K_p (3.08×10^4 or 8.41×10^4, from the partition and saturation studies, respectively) values, and considering γ_L as 0.763 M^{-1} (50), this equation leads to MIC values of 2 or 5 μM, depending on the selected K_p. These values are consistent with the antibacterial activity displayed by BP100, which inhibited in vitro growth of the bacteria *E. amylovora*, *X. vesicatoria*, and *P. syringae* at 2.5–7.5 μM (38). In addition to validating the obtained values for K_p and σ, these results strongly support the correlation between these constants and the MIC, evidencing the importance of the saturation point in the mode of action of this peptide.

Physiological significance of saturation-induced activity

The obtained results clearly point toward the occurrence of different membrane-disrupting events as saturation is reached. Given the plausible correlation between saturation and the onset of antibacterial activity of BP100, an extrapolation of these events to an in vivo setting was sought.

Surface charge neutralization at saturation was found to be an important occurrence, triggering the observed vesicle aggregation, and probably being responsible for the destabilization that led to an increase in membrane permeabilization, as leakage enhancement correlates with vesicle aggregation. The bacterial metabolism will certainly be sensitive to the neutralization-induced loss of the membrane surface potential, as this will disturb the charge environment of the outer leaflet proteins. The observed coupled permeabilization (if not lysis) entails even further damage to the cell, namely the dissipation of the transmembrane potential which, among other effects, will halt ATP synthesis. Vesicle aggregation may not have a parallel in vivo, as bacterial membranes have additional layers of protection (LPS, peptidoglycan, capsule) preventing direct membrane contact between bacteria; its occurrence in vitro does, however, stress the importance of the surface potential for membrane stability. The observed translocation could be a consequence of the permeabilization or can be an independent event; either way, direct interaction with cytoplasmic targets is yet another possible cause of bacterial death.

Effects of BP100 exposure on cell viability

The experimental results from our studies show cytotoxic effects in the cultured mammalian fibroblast cells at

concentrations of BP100 above 50–60 μM (Fig. 9). This is in good agreement with similar findings in human erythrocytes (38), where an increased release of hemoglobin was observed above 150 μM. Although the membrane integrity in our V79 cells was affected at lower concentrations (IC_{50} = 51.1 μM), it probably just reflects the different cell lines: different sensibilities to antibacterial peptides were also found between human erythrocytes and mammalian COS-7 kidney cells (65), and might indicate a better resistance of the human erythrocytes to this class of peptides (78). Results from the MTT assay (Fig. 9) demonstrated changes in the metabolic activity of mitochondria V79 cells, as the dehydrogenase enzymes started to be less active to convert the yellow water-soluble salt into insoluble formazan crystals at increasing peptide concentrations. Whether this means that there is a direct action on the mitochondria, or indirect loss of mitochondrial activity, cannot be ascertained without further investigation.

A successful application of this peptide as a bactericide demands a high therapeutic index, i.e., a high antimicrobial activity but low cytotoxicity. The high antimicrobial potency (MIC = 2.5–7.5 μM) and relatively low cytotoxicity in human erythrocytes (38) reveals promising values for BP100. Although cytotoxic effects were observed in V79 cells at peptide concentrations above 50–60 μM, this range is still far above the anticipated antimicrobial application levels.

Cytotoxicity against mammalian models is reached at a concentration higher than the MIC by roughly the same proportion that K_p values toward mammalian model bilayers are lower than toward bacterial ones. This observation suggests that cell killing may be dependent on a constant local membrane-bound concentration, independently of the considered lipid system.

CONCLUSION

This work clearly points out a correlation between high membrane concentrations (possibly even saturation) of BP100 and bacterial death. Three different potential causes of activity of AMP, i.e., charge neutralization, permeabilization, and translocation, were identified. In addition, a concentration dependence of the killing phenomena, in bacteria and in mammalian cells, was suggested. While the exact mechanism of action of the peptide may remain elusive in vivo, and depend on the peptide and bacteria species, our findings unravel the bases of the closely coupled occurrence of those causes, as experimentally observed by Friedrich et al. (79).

Fundação para a Ciência e a Tecnologia (Portugal) is acknowledged for a grant to M.N.M. (No. SFRH/BD/24778/2005). R.F. is the recipient of a predoctoral fellowship from the Ministry of Education and Science of Spain. This work was supported by grants from the Ministry of Education and Science of Spain (No. AGL2006-13564/AGR), and from the Catalan Government (No. 2005SGR00275).

REFERENCES

1. Brogden, K. A., M. Ackermann, P. B. McCray, Jr., and B. F. Tack. 2003. Antimicrobial peptides in animals and their role in host defenses. *Int. J. Antimicrob. Agents.* 22:465–478.
2. Bulet, P., R. Stocklin, and L. Menin. 2004. Antimicrobial peptides: from invertebrates to vertebrates. *Immunol. Rev.* 198:169–184.
3. Ganz, T., and R. I. Lehrer. 1998. Antimicrobial peptides of vertebrates. *Curr. Opin. Immunol.* 10:41–44.
4. Garcia-Olmedo, F., A. Molina, J. M. Alamillo, and P. Rodriguez-Palenzuela. 1998. Plant defense peptides. *Biopolymers.* 47:479–491.
5. Otvos, L., Jr. 2000. Antibacterial peptides isolated from insects. *J. Pept. Sci.* 6:497–511.
6. Zasloff, M. 2002. Antimicrobial peptides of multicellular organisms. *Nature.* 415:389–395.
7. Broekaert, W. F., B. P. A. Cammue, M. F. C. DeBolle, K. Thevissen, G. W. DeSamblanx, et al. 1997. Antimicrobial peptides from plants. *Crit. Rev. Plant Sci.* 16:297–323.
8. Hancock, R. E., and A. Patrzykat. 2002. Clinical development of cationic antimicrobial peptides: from natural to novel antibiotics. *Curr. Drug Targets Infect. Disord.* 2:79–83.
9. Hancock, R. E., and H. G. Sahl. 2006. Antimicrobial and host-defense peptides as new anti-infective therapeutic strategies. *Nat. Biotechnol.* 24:1551–1557.
10. Boman, H. G. 2003. Antibacterial peptides: basic facts and emerging concepts. *J. Intern. Med.* 254:197–215.
11. Hancock, R. E. 2001. Cationic peptides: effectors in innate immunity and novel antimicrobials. *Lancet Infect. Dis.* 1:156–164.
12. Jenssen, H., P. Hamill, and R. E. Hancock. 2006. Peptide antimicrobial agents. *Clin. Microbiol. Rev.* 19:491–511.
13. Montesinos, E. 2007. Antimicrobial peptides and plant disease control. *FEMS Microbiol. Lett.* 270:1–11.
14. Zhang, L., and T. J. Falla. 2006. Antimicrobial peptides: therapeutic potential. *Expert Opin. Pharmacother.* 7:653–663.
15. Brogden, K. A. 2005. Antimicrobial peptides: pore formers or metabolic inhibitors in bacteria? Nat. Rev. Microbiol. 3:238–250.
16. Yeaman, M. R., and N. Y. Yount. 2003. Mechanisms of antimicrobial peptide action and resistance. *Pharmacol. Rev.* 55:27–55.
17. Perron, G. G., M. Zasloff, and G. Bell. 2006. Experimental evolution of resistance to an antimicrobial peptide. *Proc. Biol. Sci.* 273:251–256.
18. Shai, Y. 2002. Mode of action of membrane active antimicrobial peptides. *Biopolymers.* 66:236–248.
19. Tossi, A., L. Sandri, and A. Giangaspero. 2000. Amphipathic, α-helical antimicrobial peptides. *Biopolymers.* 55:4–30.
20. Bechinger, B. 2004. Structure and function of membrane-lytic peptides. *Crit. Rev. Plant Sci.* 23:271–292.
21. Yang, L., T. A. Harroun, T. M. Weiss, L. Ding, and H. W. Huang. 2001. Barrel-stave model or toroidal model? A case study on melittin pores. *Biophys. J.* 81:1475–1485.
22. Shai, Y. 1999. Mechanism of the binding, insertion and destabilization of phospholipid bilayer membranes by α-helical antimicrobial and cell non-selective membrane-lytic peptides. *Biochim. Biophys. Acta.* 1462:55–70.
23. Kobayashi, S., A. Chikushi, S. Tougu, Y. Imura, M. Nishida, et al. 2004. Membrane translocation mechanism of the antimicrobial peptide buforin 2. *Biochemistry.* 43:15610–15616.
24. Hultmark, D., A. Engstrom, H. Bennich, R. Kapur, and H. G. Boman. 1982. Insect immunity: isolation and structure of cecropin D and four minor antibacterial components from *Cecropia pupae*. *Eur. J. Biochem.* 127:207–217.
25. Hultmark, D., H. Steiner, T. Rasmuson, and H. G. Boman. 1980. Insect immunity. Purification and properties of three inducible bactericidal proteins from hemolymph of immunized pupae of *Hyalophora cecropia*. *Eur. J. Biochem.* 106:7–16.

26. Sato, H., and J. B. Feix. 2006. Peptide-membrane interactions and mechanisms of membrane destruction by amphipathic α-helical antimicrobial peptides. *Biochim. Biophys. Acta.* 1758:1245–1256.
27. Andreu, D., R. B. Merrifield, H. Steiner, and H. G. Boman. 1983. Solid-phase synthesis of cecropin A and related peptides. *Proc. Natl. Acad. Sci. USA.* 80:6475–6479.
28. Steiner, H., D. Hultmark, A. Engstrom, H. Bennich, and H. G. Boman. 1981. Sequence and specificity of two antibacterial proteins involved in insect immunity. *Nature.* 292:246–248.
29. Alberola, J., A. Rodriguez, O. Francino, X. Roura, L. Rivas, et al. 2004. Safety and efficacy of antimicrobial peptides against naturally acquired *Leishmaniasis*. *Antimicrob. Agents Chemother.* 48:641–643.
30. Andreu, D., J. Ubach, A. Boman, B. Wahlin, D. Wade, et al. 1992. Shortened cecropin A-melittin hybrids. Significant size reduction retains potent antibiotic activity. *FEBS Lett.* 296:190–194.
31. Boman, H. G., D. Wade, I. A. Boman, B. Wahlin, and R. B. Merrifield. 1989. Antibacterial and antimalarial properties of peptides that are cecropin-melittin hybrids. *FEBS Lett.* 259:103–106.
32. Cavallarin, L., D. Andreu, and B. San Segundo. 1998. Cecropin A-derived peptides are potent inhibitors of fungal plant pathogens. *Mol. Plant Microbe Interact.* 11:218–227.
33. Chicharro, C., C. Granata, R. Lozano, D. Andreu, and L. Rivas. 2001. N-terminal fatty acid substitution increases the leishmanicidal activity of CA(1–7)M(2–9), a cecropin-melittin hybrid peptide. *Antimicrob. Agents Chemother.* 45:2441–2449.
34. Giacometti, A., O. Cirioni, W. Kamysz, G. D'Amato, C. Silvestri, et al. 2004. In vitro activity and killing effect of the synthetic hybrid cecropin A-melittin peptide CA(1–7)M(2–9)NH_2 on methicillin-resistant nosocomial isolates of *Staphylococcus aureus* and interactions with clinically used antibiotics. *Diagn. Microbiol. Infect. Dis.* 49:197–200.
35. Lee, D. G., Y. Park, I. Jin, K. S. Hahm, H. H. Lee, et al. 2004. Structure-antiviral activity relationships of cecropin A-magainin 2 hybrid peptide and its analogues. *J. Pept. Sci.* 10:298–303.
36. Wade, D., D. Andreu, S. A. Mitchell, A. M. Silveira, A. Boman, et al. 1992. Antibacterial peptides designed as analogs or hybrids of cecropins and melittin. *Int. J. Pept. Protein Res.* 40:429–436.
37. Ali, G. S., and A. S. Reddy. 2000. Inhibition of fungal and bacterial plant pathogens by synthetic peptides: in vitro growth inhibition, interaction between peptides and inhibition of disease progression. *Mol. Plant Microbe Interact.* 13:847–859.
38. Badosa, E., R. Ferre, M. Planas, L. Feliu, E. Besalu, et al. 2007. A library of linear undecapeptides with bactericidal activity against phytopathogenic bacteria. *Peptides.* 28:2276–2285.
39. Bardají, E., E. Montesinos, E. Badosa, L. Feliu, M. Planas, et al. 2006. Antimicrobial linear peptides. P200601098; priority date: April 28th, 2006; Oficina Española de Patentes y Marcas, Spain.
40. Ferre, R., E. Badosa, L. Feliu, M. Planas, E. Montesinos, et al. 2006. Inhibition of plant-pathogenic bacteria by short synthetic cecropin A-melittin hybrid peptides. *Appl. Environ. Microbiol.* 72:3302–3308.
41. Christensen, B., J. Fink, R. B. Merrifield, and D. Mauzerall. 1988. Channel-forming properties of cecropins and related model compounds incorporated into planar lipid membranes. *Proc. Natl. Acad. Sci. USA.* 85:5072–5076.
42. Ladokhin, A. S., M. E. Selsted, and S. H. White. 1997. Sizing membrane pores in lipid vesicles by leakage of co-encapsulated markers: pore formation by melittin. *Biophys. J.* 72:1762–1766.
43. Ladokhin, A. S., and S. H. White. 2001. ''Detergent-like'' permeabilization of anionic lipid vesicles by melittin. *Biochim. Biophys. Acta.* 1514:253–260.
44. Silvestro, L., K. Gupta, J. N. Weiser, and P. H. Axelsen. 1997. The concentration-dependent membrane activity of cecropin A. *Biochemistry.* 36:11452–11460.
45. Steiner, H., D. Andreu, and R. B. Merrifield. 1988. Binding and action of cecropin and cecropin analogues: antibacterial peptides from insects. *Biochim. Biophys. Acta.* 939:260–266.
46. Mayer, L. D., M. J. Hope, and P. R. Cullis. 1986. Vesicles of variable sizes produced by a rapid extrusion procedure. *Biochim. Biophys. Acta.* 858:161–168.
47. Santos, N. C., and M. A. Castanho. 2002. Fluorescence spectroscopy methodologies on the study of proteins and peptides. On the 150th anniversary of protein fluorescence. *Trends Appl. Spectrosc.* 4:113–125.
48. Coutinho, A., and M. Prieto. 1993. Ribonuclease-T_1 and alcohol-dehydrogenase fluorescence quenching by acrylamide—a laboratory experiment for undergraduate students. *J. Chem. Educ.* 70:425–428.
49. Santos, N. C., M. Prieto, and M. A. Castanho. 2003. Quantifying molecular partition into model systems of biomembranes: an emphasis on optical spectroscopic methods. *Biochim. Biophys. Acta.* 1612:123–135.
50. Nagle, J. F., and M. C. Wiener. 1988. Structure of fully hydrated bilayer dispersions. *Biochim. Biophys. Acta.* 942:1–10.
51. Ladokhin, A. S., S. Jayasinghe, and S. H. White. 2000. How to measure and analyze tryptophan fluorescence in membranes properly, and why bother? Anal. Biochem. 285:235–245.
52. Wenk, M. R., and J. Seelig. 1998. Magainin 2 amide interaction with lipid membranes: calorimetric detection of peptide binding and pore formation. *Biochemistry.* 37:3909–3916.
53. Melo, M. N., and M. A. Castanho. 2007. Omiganan interaction with bacterial membranes and cell wall models. Assigning a biological role to saturation. *Biochim. Biophys. Acta.* 1768:1277–1290.
54. Chalpin, D. B., and A. M. Kleinfeld. 1983. Interaction of fluorescence quenchers with the *n*-(9-anthroyloxy) fatty acid membrane probes. *Biochim. Biophys. Acta.* 731:465–474.
55. Fernandes, M. X., J. Garcia de la Torre, and M. A. Castanho. 2002. Joint determination by Brownian dynamics and fluorescence quenching of the in-depth location profile of biomolecules in membranes. *Anal. Biochem.* 307:1–12.
56. Chattopadhyay, A., and E. London. 1988. Spectroscopic and ionization properties of *N*-(7-nitrobenz-2-oxa-1,3-diazol-4-yl)-labeled lipids in model membranes. *Biochim. Biophys. Acta.* 938:24–34.
57. Pokorny, A., and P. F. Almeida. 2004. Kinetics of dye efflux and lipid flip-flop induced by δ-lysin in phosphatidylcholine vesicles and the mechanism of graded release by amphipathic, α-helical peptides. *Biochemistry.* 43:8846–8857.
58. Lakowicz, J. R. 1999. Quenching of fluorescence. Principles of Fluorescence Spectroscopy, 2nd Ed. Kluwer Academic/Plenum, New York; London.
59. Gregory, S. M., A. Cavenaugh, V. Journigan, A. Pokorny, and P. F. Almeida. 2008. A quantitative model for the all-or-none permeabilization of phospholipid vesicles by the antimicrobial peptide cecropin A. *Biophys. J.* 94:1667–1680.
60. Rueff, J., C. Chiapella, J. K. Chipman, F. Darroudi, I. D. Silva, et al. 1996. Development and validation of alternative metabolic systems for mutagenicity testing in short-term assays. *Mutat. Res.* 353:151–176.
61. Zucco, F., I. De Angelis, and A. Stammati. 1998. Cellular models for in vitro toxicity testing. *In* Animal Cell Culture Techniques. M. Clynes, editor. Springer, Berlin; London.
62. Mickuviene, I., V. Kirveliene, and B. Juodka. 2004. Experimental survey of non-clonogenic viability assays for adherent cells in vitro. *Toxicol. In Vitro.* 18:639–648.
63. Mitchell, J. B. 1988. Potential applicability of nonclonogenic measurements to clinical oncology. *Radiat. Res.* 114:401–414.
64. Brink, C. B., A. Pretorius, B. P. van Niekerk, D. W. Oliver, and D. P. Venter. 2008. Studies on cellular resilience and adaptation following acute and repetitive exposure to ozone in cultured human epithelial (HeLa) cells. *Redox Rep.* 13:87–100.
65. Cudic, M., C. V. Lockatell, D. E. Johnson, and L. Otvos, Jr. 2003. In vitro and in vivo activity of an antibacterial peptide analog against uropathogens. *Peptides.* 24:807–820.
66. Scholze, M., W. Boedeker, M. Faust, T. Backhaus, R. Altenburger, et al. 2001. A general best-fit method for concentration-response curves and the estimation of low-effect concentrations. *Environ. Toxicol. Chem.* 20:448–457.

67. Zhao, H., R. Sood, A. Jutila, S. Bose, G. Fimland, et al. 2006. Interaction of the antimicrobial peptide pheromone Plantaricin A with model membranes: implications for a novel mechanism of action. *Biochim. Biophys. Acta.* 1758:1461–1474.

68. Huang, H. W. 2000. Action of antimicrobial peptides: two-state model. *Biochemistry.* 39:8347–8352.

69. Huang, H. W. 2006. Molecular mechanism of antimicrobial peptides: the origin of cooperativity. *Biochim. Biophys. Acta.* 1758:1292–1302.

70. Segrest, J. P., H. De Loof, J. G. Dohlman, C. G. Brouillette, and G. M. Anantharamaiah. 1990. Amphipathic helix motif: classes and properties. *Proteins.* 8:103–117.

71. Kandasamy, S. K., and R. G. Larson. 2006. Molecular dynamics simulations of model trans-membrane peptides in lipid bilayers: a systematic investigation of hydrophobic mismatch. *Biophys. J.* 90:2326–2343.

72. Abrunhosa, F., S. Faria, P. Gomes, I. Tomaz, J. C. Pessoa, et al. 2005. Interaction and lipid-induced conformation of two cecropin-melittin hybrid peptides depend on peptide and membrane composition. *J. Phys. Chem. B.* 109:17311–17319.

73. Juvvadi, P., S. Vunnam, E. L. Merrifield, H. G. Boman, and R. B. Merrifield. 1996. Hydrophobic effects on antibacterial and channel-forming properties of cecropin A-melittin hybrids. *J. Pept. Sci.* 2:223–232.

74. Rathinakumar, R., and W. C. Wimley. 2008. Biomolecular engineering by combinatorial design and high-throughput screening: small, soluble peptides that permeabilize membranes. *J. Am. Chem. Soc.* 130:9849–9858.

75. Henriques, S. T., M. N. Melo, and M. A. Castanho. 2007. How to address CPP and AMP translocation? Methods to detect and quantify peptide internalization in vitro and in vivo. (Review). *Mol. Membr. Biol.* 24:173–184.

76. Matsuzaki, K., S. Yoneyama, O. Murase, and K. Miyajima. 1996. Transbilayer transport of ions and lipids coupled with mastoparan X translocation. *Biochemistry.* 35:8450–8456.

77. Persson, D., P. E. Thoren, and B. Norden. 2001. Penetratin-induced aggregation and subsequent dissociation of negatively charged phospholipid vesicles. *FEBS Lett.* 505:307–312.

78. Otvos, L., Jr., K. Bokonyi, I. Varga, B. I. Otvos, R. Hoffmann, et al. 2000. Insect peptides with improved protease-resistance protect mice against bacterial infection. *Protein Sci.* 9:742–749.

79. Friedrich, C. L., D. Moyles, T. J. Beveridge, and R. E. Hancock. 2000. Antibacterial action of structurally diverse cationic peptides on Gram-positive bacteria. *Antimicrob. Agents Chemother.* 44:2086–2092.